HANSER

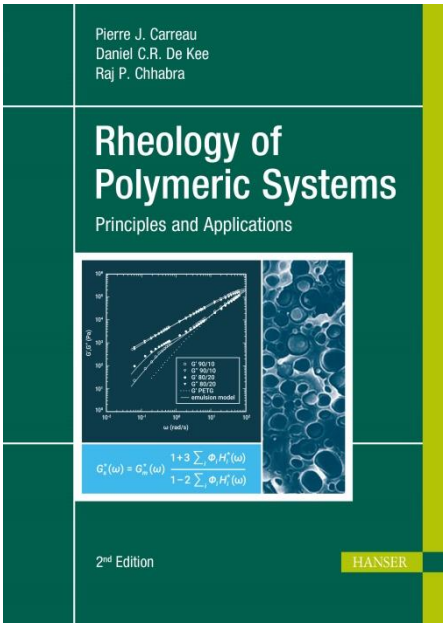

Sample Pages

Rheology of Polymeric Systems

Pierre J. Carreau, Daniel C. R. De Kee and Raj P. Chhabra

ISBN (Book): 978-1-56990-722-1
ISBN (E-Book): 978-1-56990-723-8

For further information and order see

www.hanserpublications.com (in the Americas)

www.hanser-fachbuch.de (outside the Americas)

Preface

It is almost 25 years since the first edition of this book was published. On the one hand, the fact that this title has continued to be consulted by readers testifies to the timelessness and continued relevance of the material covered in this book. On the other hand, 25 years is a rather long time in any discipline and it is thus deemed appropriate to prepare a revised and updated edition of this work. The philosophy and objective of this edition continue to be the same as that of the first edition, namely, to develop a text book for graduate and/or advanced year undergraduate students in the diverse disciplines of chemical and food engineering, mechanical engineering, material science, and polymer and plastics technology, to mention a few.

Rheology continues to be an important field of research and it finds applications in a variety of industrial sectors such as polymers, foods, cosmetics, paints, healthcare and pharmaceuticals, waste disposal of mine tailings, and biological and biomedical engineering related products and processes. Some of the currently available books cover the new trends in research very well, while only a few books address the applications. This book intends to bridge the gap between fundamental concepts and applications. The bulk of the material presented here has been used successfully for many years in our respective courses.

This book is designed to be used as a textbook for a graduate or advanced undergraduate course in polymer rheology. The level is between that of introductory texts and of highly advanced research monographs. We consider the introduction of a treatment of rheology at this level to be very timely, for few of the existing books bring together the fundamentals and applications of rheology. This work aims to develop a systematic approach and a clear understanding of the envisaged applications. The reader is expected to be familiar with introductory transport phenomena, or equivalent fluid mechanics and heat and mass transfer.

The organization of this book is as follows. The text introduces the subject of rheology via the description of unusual phenomena such as rod climbing, extrudate swell, stable bubble shapes, segregation of particles in viscoelastic fluids, migration of particles across the streamlines, etc. In Chapter 2, material functions are

defined for a variety of flow situations. Generalized Newtonian fluid models are introduced, and their predictions are compared to typical experimental data for real materials. Chapter 3 deals with the subject of rheometry. Measurements of viscosity, normal stress differences, elongational viscosity, complex viscosity, and yield stress, using capillary, concentric cylinder, and cone-and-plate geometries, are reviewed in detail. Included here is also a detailed section on the measurement of yield stress. Isothermal flows, as well as heat and mass transfer in simple geometries involving generalized non-Newtonian fluids, are dealt with in Chapter 4. The subject of linear viscoelasticity is discussed in Chapter 5, whereas Chapter 6 reviews the area of nonlinear deformation and the formulation of appropriate constitutive equations. The molecular approach to the modeling is dealt with in an introductory fashion in Chapter 7, and topics dealing with the rheology of suspensions and immiscible polymer blends, and flow characteristics of non-Newtonian media involving bubbles, drops, and particles, are discussed in Chapter 8, and mixing of complex fluids in Chapter 9. Finally, we present a substantial appendix (Chapter 10) dealing with tensor analysis, which is largely based on a text on advanced mathematics. The material presented in the first five chapters can be used as an introduction to the subject. A more advanced course would also encompass Chapters 6, 7, and 10, while Chapters 8 and 9 focus on major areas of applications. In addition to the general overall updating of the contents, the specific changes made in this edition are briefly summarized here: extensive discussion on the available methods for the measurement of yield stress (Section 3.5.1); a new section (Section 4.6) on non-Fickian diffusion and the its consequences on mass transport in structured fluids; an extended section on the linear viscoelasticity of polymer blends (Section 8.2.3); rheology of glass fiber reinforced systems (Section 8.2.5); and significantly expanded discussion on the rheology of suspensions of interactive particles (Section 8.2.6).

Like in the case of the first edition, while making changes in this edition, we have been strongly inspired by the monumental book *Transport Phenomena* (Bird, Stewart, and Lightfoot, 1960, 2006) and by *Dynamics of Polymeric Liquids,* especially Volume I (Bird, Armstrong, and Hassager, 1977, 1987). While we do not try to match the in-depth coverage of *Dynamics of Polymeric Liquids,* we present results of our extensive teaching and research experience in this field in a coherent manner, especially from the students' perspective. In this regard, this book has a distinct engineering flavor, covering topics such as mixing and flow of particulate systems, which are seldom discussed in other books on rheology. Furthermore, statements such as *"it can easily be shown"* have carefully been avoided as far as possible, in favor of a fair amount of detailed explanation. Several homework problems appear at the end of most chapters. These problems are labeled by a superscript a or b indicating the level of difficulty. The "b-problems" are the more demanding ones.

In preparing this book, we have made extensive use of the research literature and research performed in our respective laboratories by our graduate students and research associates over the past 40–50 years. Special thanks go to Drs. C. F. Chan Man Fong and M. Grmela, who contributed to many facets of the first edition of this book. We acknowledge also the devotion of Ms. D. Heroux, who patiently typed and re-typed what must have seemed endless revisions of the first edition. We are thankful to Mr. F. St-Louis and Dr. N. Chapleau for preparing the artwork for the first edition and which was largely used in this second edition. We acknowledge the help of Dr. Chen Feng in preparing some chapters of the second edition. Finally, we are grateful to Dr. David Barden of Clearly Scientific who edited this second edition, suggesting improvements and signaling numerous corrections.

P. J. Carreau

D. De Kee

Raj P. Chhabra

Contents

1 Introduction

Because science evolved and developed first through experimentation, it is appropriate to introduce the complex field of rheology by discussing some of the intriguing and paradoxical phenomena encountered with polymeric liquids and some particulate suspensions. A similar presentation can be found in most textbooks on rheology. For this reason, we have restricted the number of such examples in this chapter. Some definitions and a classification are presented first.

1.1 Definitions and Classification

Rheology is a science that deals with the deformation of materials as a result of an applied stress. It can therefore be considered part of continuum mechanics, although it is also possible to relate the stress to the deformation or to the rate of deformation via molecular kinetic theory.

Two physical laws dating back to the seventeenth century are very important in the present context. They are:

I. *Hooke's law,* describing the behavior of an elastic solid, given in shear by

$$\sigma_{yx} = -G\frac{du_x}{dy}, \tag{1.1}$$

where the shear stress σ_{yx} (see Chapter 2) is related to the deformation gradient du_x/dy via the constant elastic modulus G.

II. *Newton's law,* describing the behavior of a linear viscous fluid, given by

$$\sigma_{yx} = -\mu\frac{dV_x}{dy}, \tag{1.2}$$

where the shear stress σ_{yx} is related to the rate of deformation dV_x/dy, via the constant Newtonian viscosity μ.

We can consider two limiting cases of material response: that of a non-deformable body on the one hand and that of an inviscid fluid on the other hand. For a non-deformable body, the elastic modulus is infinite. For an inviscid fluid, the viscosity is zero.

The behavior of real materials falls between these limiting situations. Table 1.1 summarizes the observed rheological behavior. For instance, we can say that although most real materials have a finite viscosity, under certain conditions (e.g., flow of air over an aerofoil), the effect of viscosity is confined to a thin layer (boundary layer, see Section 4.5). Beyond this, the fluid behavior can be well-represented by an ideal inviscid fluid. However, in most confined flow situations, the effects of viscosity cannot be ignored. At the other extreme is an ideal elastic material which attains an equilibrium deformation when subjected to an external stress. For some materials, these limiting behaviors are easily observed. In contrast, the viscosity of ice or the elasticity of water may go unnoticed! In between these two extremes, the fluid behavior gradually passes from inviscid ideal to viscous, to viscoelastic fluid-like, to solid-like, and then to an elastic solid, as summarized schematically in Table 1.1.

Many of the terms used in the field of rheology have been carefully defined by Lodge (1964). We summarize here some of the important definitions.

Table 1.1 Summary of Rheological Behavior

Continuum mechanics	Fluids	Inviscid fluid (ideal case with $\mu = 0$)	None
		Linear viscous fluid (Newtonian behavior)	Water
		Non-linear viscous material (generalized Newtonian behavior defined in Section 1.2)	Suspensions in Newtonian media
		Linear viscoelastic material	Polymer under small deformation
		Non-linear viscoelastic material	Concentrated polymer solutions or plastics under large deformation
	Solids	Non-linear elastic material	Rubber
		Linear elastic solid	Linear Hookean spring
		Non-deformable solid (ideal case with $G = \infty$)	None

1.1.1 Purely Viscous or Inelastic Material

A material is purely viscous or inelastic if, following any flow or deformation history: (a) the stresses in the material become instantaneously zero (or isotropic) as soon as the flow is stopped (deformation rate set to zero); or (b) the deformation rate (in the absence of inertial effects) becomes instantaneously zero when the stresses are set equal to zero (or are isotropic).

1.1.2 Perfectly Elastic Material

A material is perfectly elastic if the equilibrium shape is attained instantaneously when non-isotropic stresses are applied, or if the stresses become non-isotropic as soon as the material is deformed. Hooke's law (Equation 1.1) describes a perfectly linear elastic body, if the modulus G is considered constant. The behavior of a rubber band approximates closely that of a perfectly elastic body, but a highly non-linear one, since in this case the modulus changes with deformation.

1.1.3 Viscoelastic Material

Any material which obeys neither the purely viscous nor the perfectly elastic criteria is viscoelastic. The parts of the word, *viscous* and *elastic,* describe a rheological behavior between that of a purely viscous liquid and that of a perfectly elastic solid. In simple terms, a viscoelastic material will not deform instantaneously when non-isotropic stresses are applied, or the stresses will not respond instantaneously to any imposed deformation or deformation rate. Typical examples are polymer solutions and plastics that are known to exhibit memory effects such as relaxation, described in Chapter 2. The phenomena described in Section 1.2 are mostly due to viscoelasticity.

■ 1.2 Non-Newtonian Phenomena

Most polymer systems, as well as many other complex fluids, do not obey Newton's law of viscosity. These fluids generally exhibit a viscosity that decreases with increasing rate of deformation. This is referred to as pseudoplastic or shear-thinning behavior. Very large decreases in viscosity are observed in polymeric fluids, as illustrated in Chapter 2. Moreover, polymeric fluids have a viscoelastic character that is responsible for a number of spectacular phenomena not observed with New-

tonian fluids. The design of many industrial processing operations requires taking into account several of these phenomena.

We review here some of the more striking viscoelastic effects. An excellent presentation of rheological or non-Newtonian phenomena can be found in the books of Bird, Armstrong, and Hassager (Volume 1, 1977 or 1987) and in another book by Boger and Walters (1993). In writing the following sections we have been largely inspired by these authors.

1.2.1 The Weissenberg Effect

This phenomenon is illustrated schematically in Figure 1.1. If a rod is rotated in a beaker containing a Newtonian fluid such as water, the free surface is deformed by a centrifugal force, creating a vortex in the center. In contrast, if a rod is rotated in a polymer solution or melt, the fluid tends to climb the rod, and an inverted vortex is created. Weissenberg (1947) was able to explain this phenomenon in terms of unequal normal stresses present in such materials under steady shearing conditions (see Section 3.2.3).

The polymer molecules in a solution or melt form an entangled network, which, when deformed in one direction through the action of a rotating or moving surface, generates internal tensions in the flow direction as well as normal to the flow direction. These tensions are the normal stresses mentioned in the previous paragraph. In fact, if we could measure the pressure at point A on the rod and at point B on the beaker, we would observe, contrary to the Newtonian case, that with the polymeric fluid, $P_A > P_B$. This excess pressure is compensated by an extra hydrostatic head.

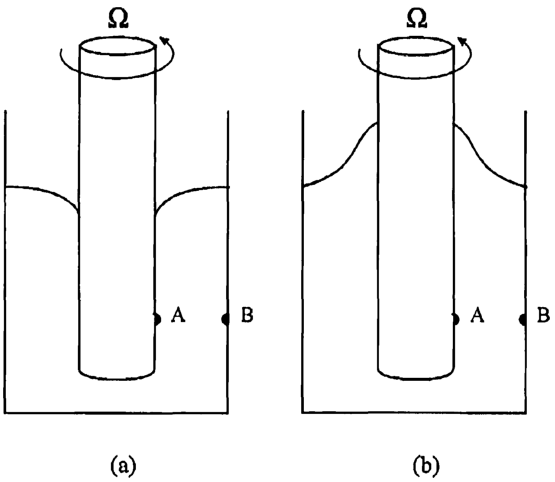

Figure 1.1
Shape of the liquid's free surface for a rotating rod in a reservoir
(a) Newtonian liquid
(b) viscoelastic liquid

1.2.2 Entry Flow, Extrudate Swell, Melt Fracture, and Vibrating Jet

Flow visualization of the entry flow in the case of a sudden contraction is illustrated in Figure 1.2. Depending on the liquid rheology and flow conditions, two main patterns are observed. The pattern of Figure 1.2 is observed for branched polymer melts such as low-density polyethylene (LDPE), polystyrene (PS), and polymethyl methacrylate (PMMA). The pattern of Figure 1.2 is typical of linear polymer melts such as high-density polyethylene (HDPE) and linear low-density polyethylene (LLDPE), as well as Newtonian fluids at low Reynolds numbers.

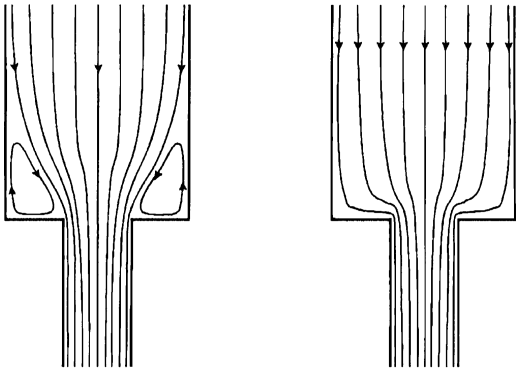

Figure 1.2
Main flow patterns in sudden contraction flow

The size of the vortices observed for LDPE, PS, etc. (Figure 1.2a) increases first with flow rate and eventually becomes unstable. The unstable flow in the reservoir appears at the same moment as the helical distortion illustrated in Figure 1.4. This has been reported by several authors (Den Otter, 1970, 1971; Ballenger et al., 1971; Boger and Ramamurthy, 1972). For linear polyethylenes, the corner vortices are usually not observed, and the flow pattern is that shown in Figure 1.2b.

Another spectacular observation that is very important in the transformation of plastics is the swell of the extrudate as it emerges from a capillary. This is shown in Figure 1.3. A Newtonian fluid (C) normally shows a small decrease (< 20%) in diameter as it emerges from the capillary. This is due to inertial effects. In contrast, a highly elastic fluid (A), such as a polymer melt, could show a 200% to 400% increase in diameter. This extrudate swell effect is very frequently referred to in the literature as the *die swell* effect. For obvious reasons this terminology should be avoided!

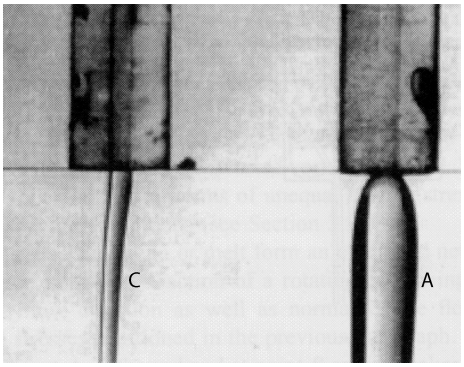

Figure 1.3
Fluid extrudates from capillary tubes
A stream of a Newtonian silicone fluid shows no diameter increase (C); a solution of 2.44 g of polymethyl methacrylate (M_n= 10^6 kg/kmol) in 100 mL of dimethylphthalate shows a 200% increase in diameter (A). Both fluids have a similar viscosity (From Lodge, 1964, with permission)

Qualitatively, we can explain this phenomenon through the presence of normal stresses (extra pressure) created at the wall of the capillary. As the polymeric fluid emerges from the capillary, this internal pressure is released, resulting in a lateral expansion. Another important contribution is due to memory effects in polymeric fluids that behave like rubbery materials. When entering a small capillary die from a large reservoir, the fluid is subjected to a rapid change of shape (large deformation), and as it emerges from the die, it tends through its rubbery nature to recover its initial shape (elastic recovery). For this reason, polymeric fluids are often referred to as fluids with memory. Other effects, such as velocity changes at the exit and thermal gradients in the extrudate, also contribute to this phenomenon (Tanner, 2000).

Extrudate swell is thus associated with the elastic nature of the fluid, and its measurement is frequently used to characterize polymer melt elasticity in relation to its molecular structure, molecular weight, and molecular weight distribution. Extrudate swell is a phenomenon that has to be taken into account in fiber production operations. Critical velocity gradients are also complicating and may lead to melt fracture.

Melt fracture is observed as a polymer is extruded freely from a die at a rate exceeding a critical value. The diameter of the extrudate is no longer uniform and may exhibit various distortions, all referred to as melt fracture. Figure 1.4 illustrates various shapes of melt fracture encountered under different flow conditions.

- Defects known as *sharkskin* are shown in Figure 1.4. This is an often periodic instability, which depends on the flow rate, temperature, and properties of the polymer. In (a), the extrudate is a linear low-density polyethylene (LDPE), whereas in (b), it is a high-density polyethylene (HDPE).
- In some cases, we observe smooth surfaces followed by so-called sharkskin zones. This is referred to as a bamboo effect (attributed to the stick-slip phenomenon (c)).

- As the extrusion rate is increased, the sharkskin may disappear and the surface of the extrudate may again become smooth, as shown in (d).
- Helical or screw shapes are frequently encountered in the flow of polystyrene (e) or in the flow of polypropylene (f). The amplitude of the distortions increases with increasing flow rate. As the flow rate is further increased, polyethylene, polystyrene, and polypropylene exhibit chaotic distortions (g).

Other polymers may exhibit one or more of the distortions shown in Figure 1.4.

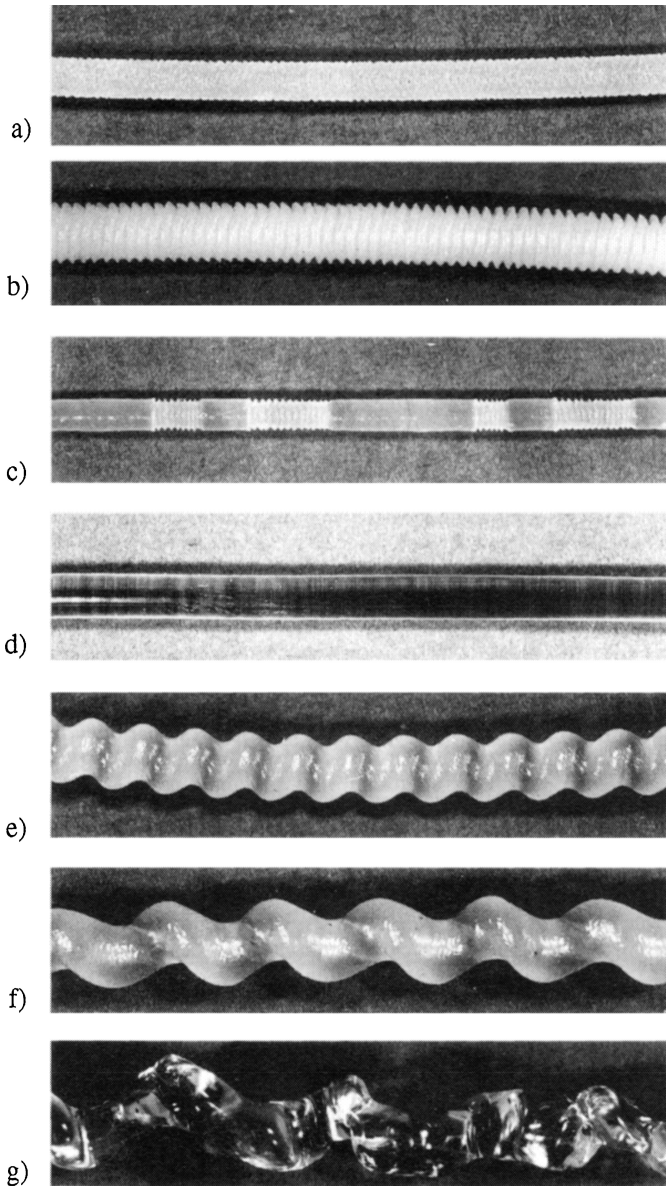

Figure 1.4
Range of shapes of extrudates under melt fracture (From Agassant et al., 1991)

Distortions similar to melt fracture have been observed in polymer processing, such as the calendering of polyvinylchloride (PVC). The film of PVC, usually transparent, becomes partly opaque, and the surface that is not in contact with the roller shows surface defects as the roller's velocity increases, or if the nip between the rollers becomes too narrow.

As a final example in this extrusion section, we show in Figure 1.5 the behavior of a jet emerging from a nozzle subjected to a transverse vibration. The Newtonian fluid (a) breaks into droplets. A concentrated polymer solution (c) emerges as a structurally stable non-uniform wave. Dilute (and very dilute) polymer solutions (b) exhibit a behavior in between. that of (a) and (c); that is, drops are connected by a thread. Chan Man Fong et al. (1993) have presented an analysis of this problem, involving elongational as well as oscillatory flow.

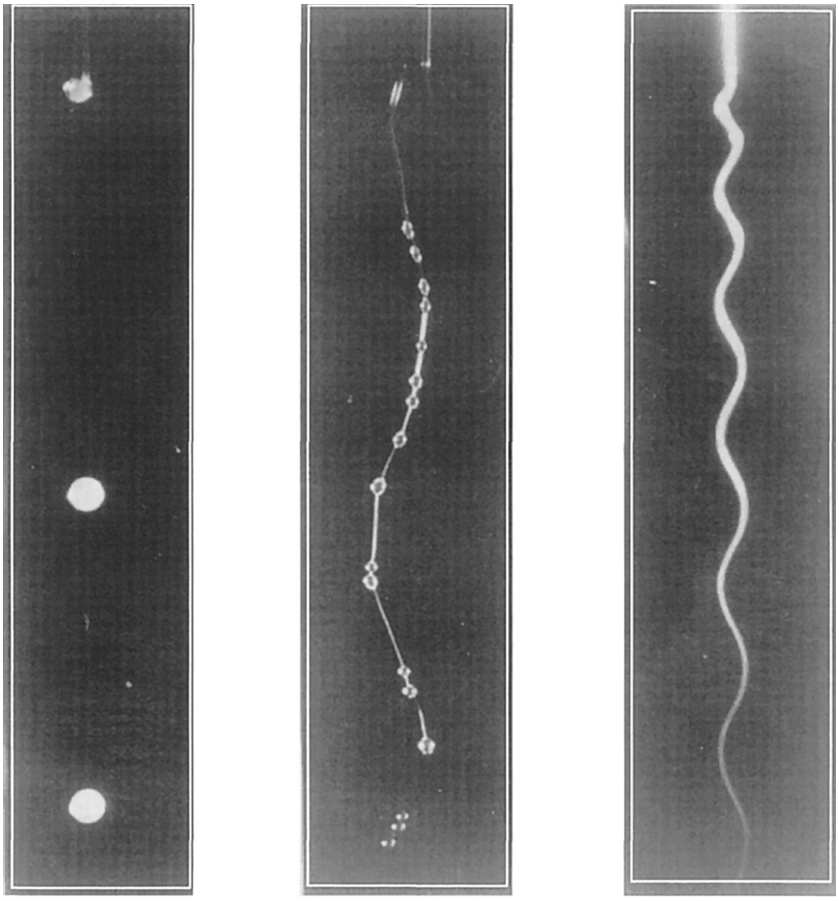

Figure 1.5 Liquid emerging from a vibrating nozzle
(a) Newtonian fluid
(b) dilute polymer solution
(c) concentrated polymer solution

1.2.3 Recoil

One experiment that may easily be performed to show the elastic nature of polymeric fluids is the following. If an elastic fluid is forced down a tube by applying a pressure gradient, the fluid will deform continuously. At a given time, the pressure gradient is set to zero, and the fluid starts to flow in the opposite direction. Photos of such an experiment can be found in the textbook of Fredrickson (1964). Recoil can be quite spectacular, as shown by Professor Lodge's experiment in Figure 1.6.

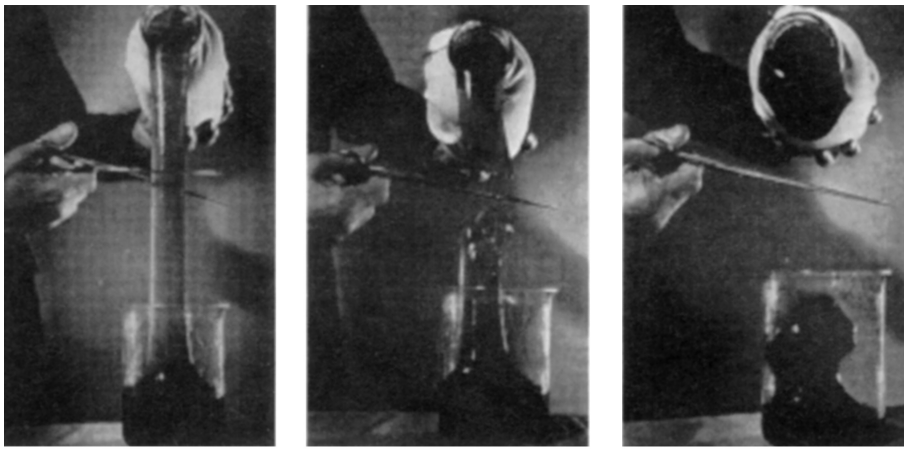

Figure 1.6 Recoil in an elastic fluid
An aluminum soap solution (aluminum dilaurate in decalin and *m*-cresol), is being poured from a beaker (a) and suddenly cut in midstream (b). In photo (c), we note that the liquid above the cut snaps back into the upper beaker (From Lodge, 1964, with permission)

This phenomenon is closely related to the behavior of an elastic band when released of its tension. For viscoelastic fluids, recoil is only partial and takes a finite time. Viscoelastic fluids are said to have a "fading memory", in the sense that they are more affected by a recent deformation as opposed to a deformation experienced in the more distant past. Moreover, the effect is strongly dependent on the rate of deformation.

1.2.4 Open Syphon

A related experiment with recoil is the open syphon illustrated in Figure 1.7. The full beaker containing an aqueous solution of 0.75 mass% polyethylene oxide (WSR 301) is first tilted over to initiate the flow downward to the lower beaker, then it is

set back straight. The polymer solution will continue to flow against gravity (over a few cm) and downward until the upper beaker is almost empty. This open-syphon phenomenon is due to the highly elastic nature of this polymer solution, which remembers its recent state (fading memory). This flow is mostly elongational, and as discussed in Chapter 2 (Section 2.1.4), the elongational viscosity of polymer solutions can be quite large compared to their shear viscosity.

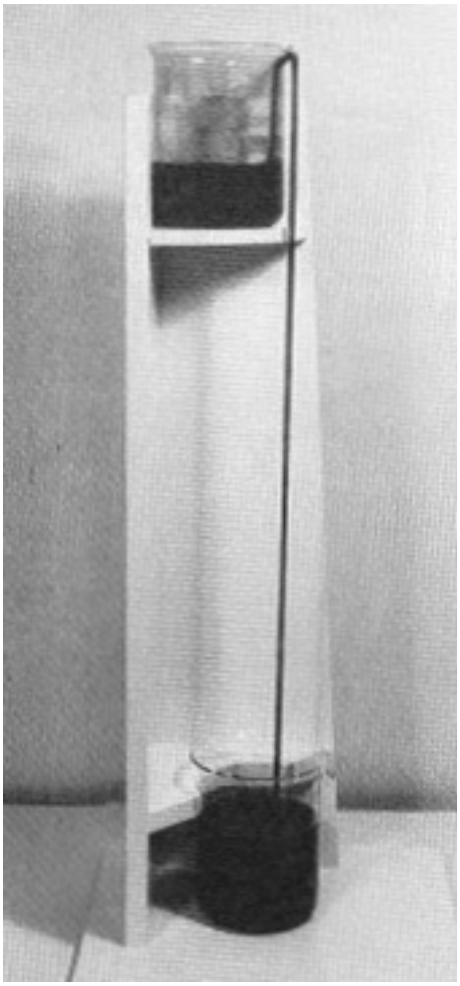

Figure 1.7
Open syphon
Open-syphon effect illustrated for an aqueous solution of 0.75 mass% polyethylene oxide, WSR 301 (From Barnes et al., 1989)

1.2.5 Antithixotropic Effect

The phenomenon of antithixotropy (sometime referred to as dilatancy) illustrated in Figure 1.8 is quite spectacular, although rarely observed compared to thixotropic effects observed for foodstuffs such ketchup, paints and other concentrated

suspensions. In the case illustrated in the figure, under vigorous shaking of an alkaline perbunan latex (which initially is very much a liquid), a structure is built up. This structure is responsible for a sudden, very large increase of its viscosity and solid-like behavior. Upon cessation of the shaking, the structure is destroyed and the latex regains after a few minutes its natural liquid-like behavior. The same phenomenon has been widely reported on youtube as the so-called "cornstarch walk on water" effect *(https://www.youtube.com/watch?v=RUMX_b_m3Js).* People are shown walking over a bathtub filled with concentrated solutions of cornstarch in water.

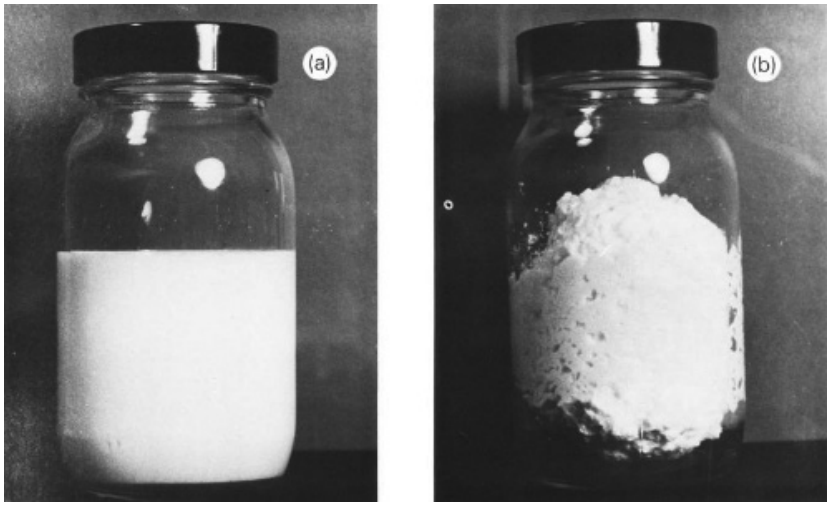

Figure 1.8 Antithixotropic effect
Antithixotropic effect demonstrated for an alkaline perbunan liquid latex. (a) shows the liquid latex at its rest state and (b) after vigorous shaking the behavior is that of a solid. On cessation of shaking the latex will regain, after a few minutes, its original state (a). (From Cheng, 1973 and Walters, 1980)

1.2.6 Drag Reduction

Most of the preceding effects are observed in the low Reynolds number regime, i.e., in the absence of inertial effects. One phenomenon that was of considerable interest in research in the 1970s is the drag reduction obtained by adding a small quantity of high molecular weight, linear, soluble polymers to a fluid in a turbulent flow regime in pipes. Figure 1.9 shows a conventional friction factor-Reynolds number plot obtained for two polymer solutions in turbulent tube flow.

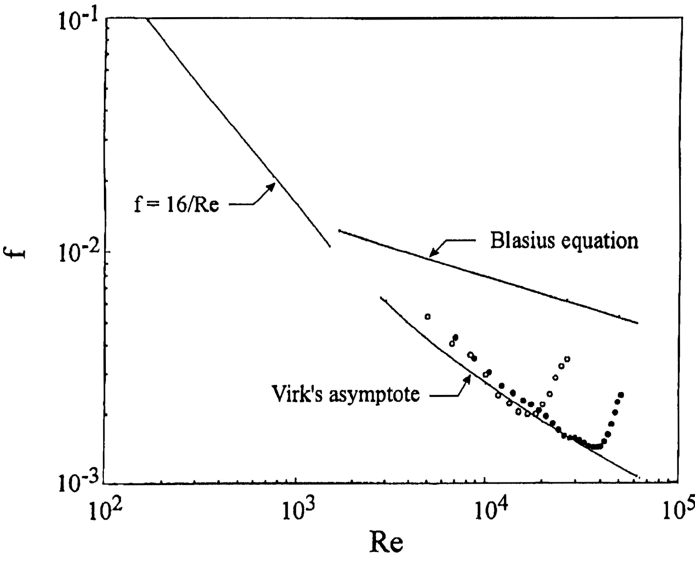

Figure 1.9 Typical drag reduction data for the turbulent flow of a 100 ppm PIB solution in cyclohexane (●) and a 100 ppm ODR solution in kerosene (○) (Adapted from Tiu et al., 1995)

The friction factor and the Reynolds number are defined by

$$f = \frac{1}{4}\left(\frac{D}{L}\right)\Delta P \Big/ \frac{1}{2}\rho\langle V\rangle^2 \tag{1.3}$$

and

$$\mathrm{Re} = \frac{D\langle V\rangle\rho}{\mu}, \tag{1.4}$$

where D and L are the tube diameter and length respectively, ΔP is the pressure drop, (V) is the average fluid velocity, and ρ and μ are the fluid density and viscosity respectively. One fluid was a solution containing 100 ppm (mass parts per million) of polyisobutylene (PIB) of a very high molecular weight (~ 2×10^6 kg/kmol) in cyclohexane. The other fluid was a 100 ppm solution of a commercial organic drag reducer (ODR) in kerosene. The molecular weight of the polymer was about 4×10^6 kg/kmol. The figure also shows the theoretical laminar result ($f = 16/\mathrm{Re}$), the empirical Blasius equation for the turbulent flow in a smooth pipe ($f = 0.0791/\mathrm{Re}^{0.25}$) for Newtonian fluids, and the Virk (1975) asymptote (also known as the maximum drag reduction, MDR) for drag-reducing fluids. Both polymer solutions exhibit a substantial reduction of the friction in the turbulent flow regime up to critical values of the Reynolds number. A reduction by a factor of about 2 with respect to the Blasius result obtained for Newtonian solvents is observed. At a critical Reynolds number depending upon the polymer soultion, the data show an upward turn, suggesting polymer degradation.

Figure 1.10 compares the drag reduction with the corresponding heat transfer reduction in turbulent flow in a tube, obtained for a 100 ppm polyacrylamide solution in water. The shear viscosity of this solution was found to be constant and slightly larger than that of water (μ = 1.2 mPa·s).

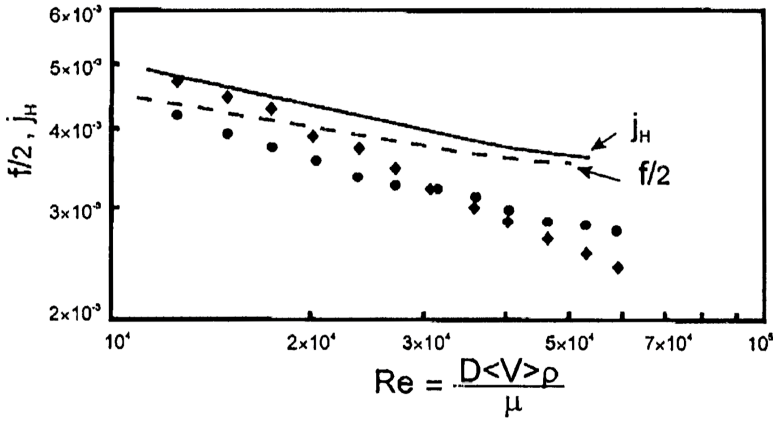

Figure 1.10 Heat transfer (–) and pressure drop data (- - -) for water in a circular pipe Friction factor (●) and heat transfer data (♦) for a 100 ppm aqueous polyacrylamide solution (From Del Villar et al., 1984)

The pressure drop and heat transfer are reported in terms of the friction factor f and the heat transfer factor j_H defined by

$$j_H = \frac{\mathrm{Nu}}{\mathrm{Re}\,\mathrm{Pr}^{1/3}} \tag{1.5}$$

The Nusselt number, Nu, and the Prandtl number, Pr, are defined by

$$\mathrm{Nu} = \frac{hD}{k} \tag{1.6}$$

and

$$\mathrm{Pr} = \frac{\hat{C}_p \mu}{k}, \tag{1.7}$$

where h is the heat transfer coefficient, and k and $\hat{C}_p$ are the fluid thermal conductivity and the heat capacity per unit mass respectively.

Although the viscosity of the polyacrylamide solution used in experiments is slightly larger than that of water, the friction factor for the polymer solution is considerably lower than the expected value for water. The heat transfer reduction when using the polymer solution is possibly more important at higher values of the Reynolds number. For highly turbulent flow conditions, we expect the Chilton–Colbum (1934) analogy to be valid, that is

$$j_H = \frac{f}{2}. \tag{1.8}$$

This is observed here for water only.

This unusual drag reduction phenomenon has initiated a series of industrial and military investigations. For example, some fire departments also attempted to make practical use of this drag reduction phenomenon, as illustrated in Figure 1.11. The "rapid" water, containing a small amount of polyethylene oxide, turns out to be slippery, and thus leads to safety problems. Well-known drag reducing polymers include polyethylene oxide and polyacrylamide with molecular weight above 10^6 kg/kmol. Reductions in friction by a factor of 2 to 5 are possible, but applications of drag reduction to pipeline transportation and marine applications are severely jeopardized by the mechanical degradation of the polymer solutions over prolonged use.

Figure 1.11 Effect of drag reduction on fire hose range (Taken from Schowalter, 1978, with permission)

There is no clear understanding of the mechanism of drag reduction. Some researchers have associated this effect with the elastic properties of the polymeric fluids. However, at low concentrations (in the range of 10 to 100 ppm), the fluids hardly exhibit any measurable elastic properties. A more acceptable explanation is that those supermacromolecules have a large hydrodynamic volume in the fluid, suppressing a considerable number of sites for the formation of eddies, thereby reducing the turbulence intensity. Also, such large molecules may get trapped at the wall, as a result of the wall roughness conditions. The resulting new surface (wall plus polymer) may be smoother than the pipe wall, reducing the pumping energy requirements.

1.2.7 Hole Pressure Error

This experiment illustrates non-Newtonian and viscoelastic effects associated with pressure measurements using pressure transducers. Typically, a wall pressure measurement, P_M, is made by taking a reading at the bottom of a well. As shown in Figure 1.12, the measured pressure gives the correct result for a Newtonian fluid (N) but is too low for the polymer solution (P). As discussed in Chapter 3, the pressure measured at the wall surface for the flow of a viscoelastic fluid is the sum of the thermodynamic pressure, P, and a normal stress component, σ_{yy}. The pressure measured at the bottom of the well, as shown in Figure 1.12, will thus be lower than that measured by a transducer, flush-mounted at the wall of the flow section.

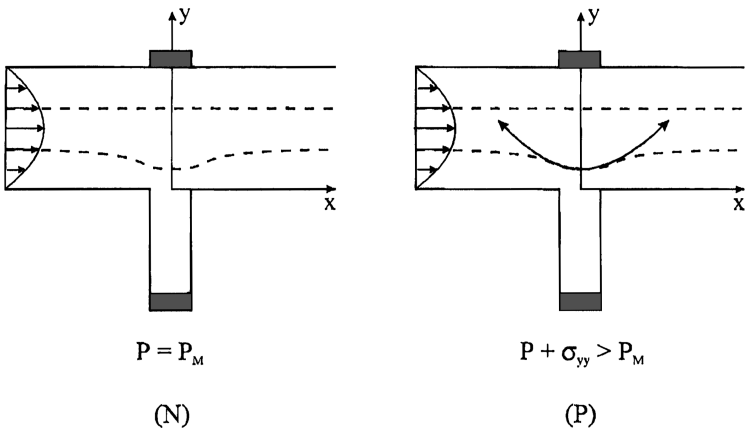

Figure 1.12 Hole pressure error
The arrows in the polymer solution indicate how an extra tension along a streamline tends to lift the fluid out of the cavity resulting in a low pressure reading (Adapted from Bird, Armstrong, and Hassager, 1987)

The hole pressure error for different geometries is related to shear and normal stresses developed in the fluid. For example, for a circular hole, the hole pressure error is associated with the shear stress, the primary normal stress difference, and the secondary normal stress difference.

While the current consensus on the secondary normal stress difference seems to be that this quantity is about ten times smaller in magnitude than the primary normal stress difference, as well as being opposite in sign, its history has been quite turbulent. In 1950, Weissenberg postulated the secondary normal stress difference to be zero. Since then, experimenters have found the secondary normal stress difference to be positive, again zero, and now negative. The fact that the magnitude of this quantity is rather small is probably a major cause of the difficulties associated with its measurement. In addition, the secondary normal stress difference is believed to have little bearing on most viscoelastic phenomena.

However, one notable exception where the secondary normal stress difference plays an important role is in the wire coating process. If, because of a disturbance, the wire finds itself off center, a force will act to bring the wire back into a central position, provided the secondary normal stress difference is negative.

1.2.8 Mixing

Non-Newtonian and elastic effects are also responsible for rather striking flow patterns associated with mixing operations. Figure 1.13 illustrates the difference in flow patterns in the vicinity of a sphere rotating in a viscoelastic solution.

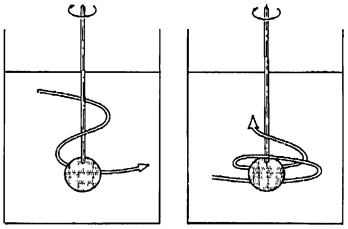

Figure 1.13
Flow patterns near a sphere rotating in a viscoelastic fluid
(a) inertial forces dominate
(b) elastic forces dominate
(From Ulbrecht and Carreau, 1985)

Another striking as well as detrimental phenomenon is the one shown in Figure 1.14. This figure illustrates the existence of stagnant zones when a polymer solution is mixed by a helical ribbon agitator. Because there is no macroscale mixing going on in a stagnant zone, a situation such as the one depicted in Figure 1.14 could be associated with extremely long mixing times, before a homogeneous product results.

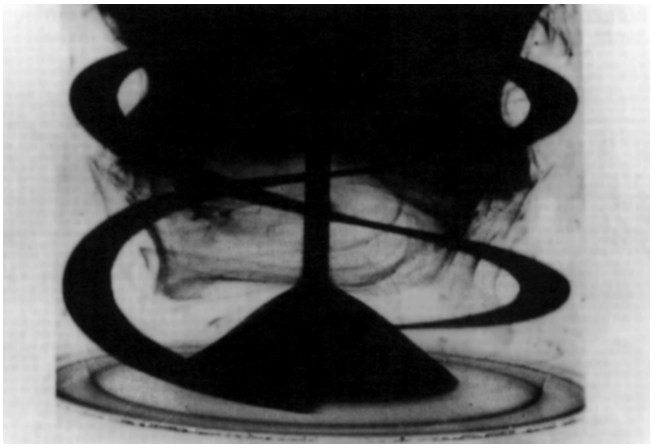

Figure 1.14 Conical stagnant zone observed in a 2 mass% aqueous solution of sodium carboxy methyl cellulose. A decoloration process is used to determine the mixing time

Keirstead et al. (1980) reported large differences in mixing effectiveness depending on the direction of rotation. They reported a difference in mixing time of one order of magnitude between rotations in the helix and counterhelix directions, when mixing ammonium nitrate gels at 200 rpm.

1.2.9 Bubbles, Spheres, and Coalescence

A variety of industrial phenomena rely on mass transfer resulting from liquid–gas contact. The shape of the bubbles is very much affected by the type of fluid. Figure 1.15 illustrates the shapes of bubbles of different volume in a viscoelastic polyacrylamide (PAA) solution and in a Newtonian glycerine solution. Different degrees of magnification were used in order to better portray the shapes, especially for the small volume bubbles. Note the striking difference in bubble shape between (c) and (d). They both portray a 1.0 mL air bubble, rising in a viscoelastic solution in (c), and in a Newtonian fluid in (d). Bubble shapes, except for very small volume bubbles, are not stable in Newtonian fluids. Several snapshots of bubbles of the same volume would result in very different pictures (De Kee and Chhabra, 1988; Chhabra, 2006). In viscoelastic fluids, the shapes are stable and vary with increasing volumes, from spherical, to a prolate teardrop, to an oblate cusped teardrop, and finally to a spherical cap shape (Chhabra and De Kee, 1992).

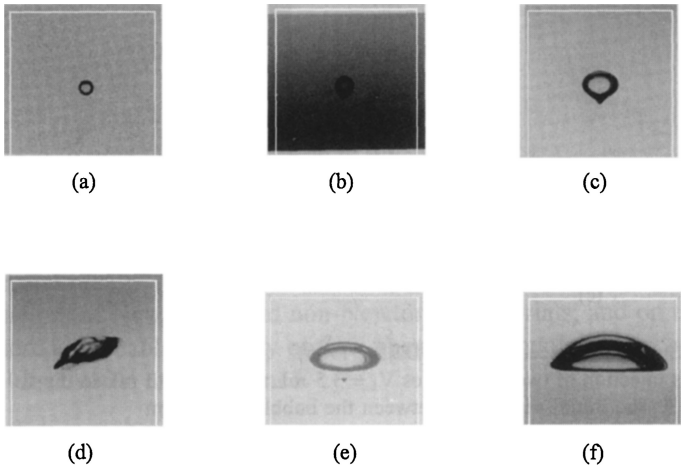

Figure 1.15 Shapes of bubbles in a polyacrylamide solution (1 mass% in a 50 mass% mixture of glycerine and water): (a) 0.01 mL; (b) 0.1 mL; (c) 1.0 mL; (e) 2.0 mL; (f) 10 mL; and (d) a 1 mL bubble in a Newtonian 40 mass% aqueous glycerine solution (From Dajan, 1985 and D. De Kee et al., 1990)

Figure 1.16 illustrates the coalescence phenomena of bubbles in a viscoelastic fluid. Photo (a) shows the simultaneous injection of two bubbles. Photos (b) and (c) illustrate the capture of the trailing bubble in the wake of the leading bubble, and then the film drainage after the bubbles make contact. Photo (d) illustrates the tremendous deformations associated with bubble capture, shown here for the simultaneous injection of three bubbles. If the time required for the film to drain and thin after bubble contact is made exceeds the period of contact, coalescence will not occur. This is usually the case for equal-volume bubbles.

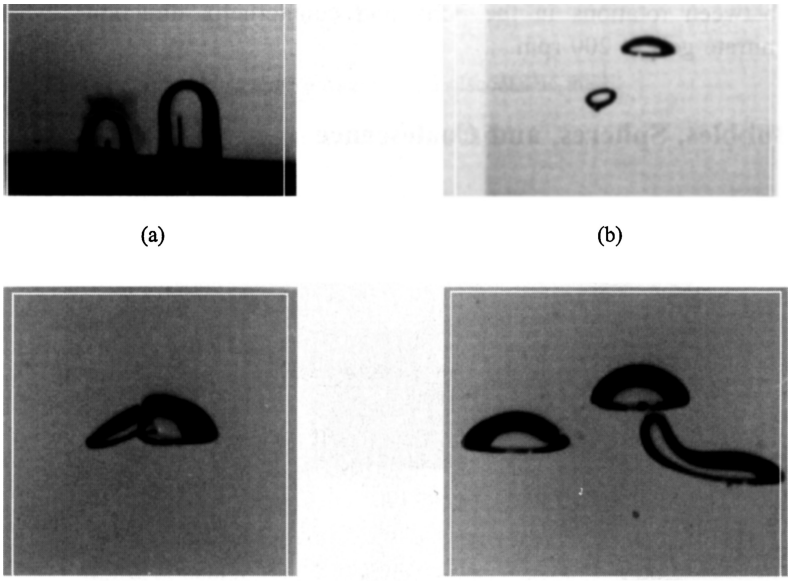

Figure 1.16 Bubble coalescence (From Dajan, 1985 and De Kee et al., 1990)
(a) Simultaneous injection of two air bubbles V_1 = 3.5 mL and V_2 = 9.3 mL in the 1.0 mass% PAA fluid of Figure 1.14. The initial separation between the bubbles is 24 mm
(b) A 1.0 mL bubble moves into the wake of a 4.7 mL bubble. The initial separation between the bubbles was 9 mm. The fluid is again the 1.0 mass% PAA fluid
(c) Bubble contact for the system in frame (b)
(d) Bubble deformation and capture following a three-bubble injection in a 1 mass% aqueous carboxy methyl cellulose solution. Each bubble had a volume of 7.5 mL and their initial separation was 30 mm

Figure 1.17 illustrates the motion of a sphere falling in a Newtonian (a) and in an elastic (b) fluid. We can observe the successive positions of the spheres. In the case of the Newtonian fluid, a constant velocity is obtained, whereas in the elastic fluid we observe a deceleration over the distance of the tube.

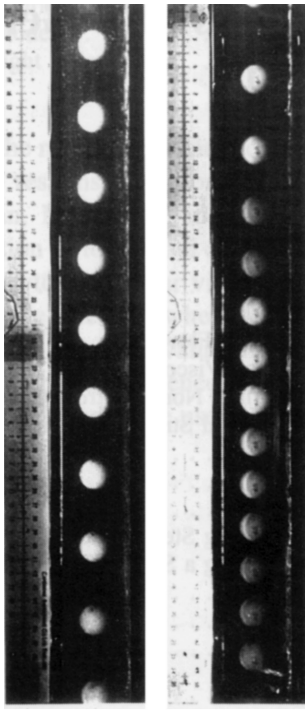

Figure 1.17
Motion of a sphere of radius 11.3 mm and density 8×10^3 kg/m^3 in a Newtonian fluid
(a) of viscosity 3 Pa·s and in an elastic Boger fluid
(b) of viscosity 3 Pa·s and relaxation time of 0.05 s
(From Jones et al., 1994, with permission)

The above are only a few examples of the different behavior exhibited by polymeric materials as compared to Newtonian fluids. We could easily discuss several more of these effects. However, the idea is on the one hand to draw attention to the striking differences between the behaviors of Newtonian and non-Newtonian materials, and on the other hand to suggest that there is probably a variety of flow phenomena involving viscoelastic liquids that is still to be discovered and explained.

2 Material Functions and Generalized Newtonian Fluids

It has been shown that even for the most complicated constitutive equations for fluids, there are special flows for which the response functional manifests itself through three viscometric functions only (Coleman, Markovitz, and Noll, 1966). A constitutive equation relates the stress to the deformation or to the rate of deformation. One of these viscometric functions is a non-linear (non-Newtonian) shear viscosity, the other two are differences of normal stresses. The answer to the question whether these viscometric functions are independent of each other is of theoretical as well as practical value. In this chapter, we define a variety of important material functions which we will encounter throughout the book. Frequently used viscosity models are presented, and some useful relations between material functions are given.

■ 2.1 Material Functions

2.1.1 Simple Shear Flow

Simple shear (viscometric) flow is defined as follows: a fluid is contained between two flat parallel plates (infinite in the x- and z-directions), as illustrated in Figure 2.1.

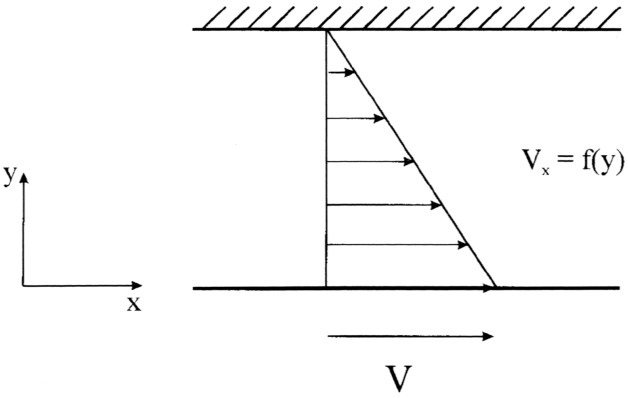

Figure 2.1 Sketch defining unidirectional shear flow

We can imagine the liquid to be composed of several thin sheets of fluid, arranged parallel to the plates. Under static conditions (both plates are stationary), the velocity profile (assuming we can talk about a velocity profile under static conditions) is represented by a vertical line. If suddenly we decide to set the lower plate in motion in the positive *x*-direction, the velocity profile may be given by the same vertical line except for a thin layer in contact with the moving plate. Fluid molecules (or particles) in this layer now will have the plate velocity, *V*, associated with their masses, and as such a different momentum.

It is now feasible for molecules to jump from layer one into the next layer and vice versa. Those molecules arriving in layer 1 will, because of the moving plate, instantly adopt the plate velocity. The molecules arriving in layer 2 (from layer 1) will increase the momentum of layer 2. Jumps occurring simultaneously in layers farther away from the moving plate do not yet affect the net change in velocity profile at this stage. The jumping process from layer to layer will result in momentum being transported in the positive *y*-direction.

Eventually, provided the gap between the plates is small enough and the flow is laminar, a linear velocity profile will be established for which we can write

$$V_x = \dot{\gamma}_{yx} y; \quad V_y = V_z = 0, \tag{2.1}$$

where the shear rate is

$$\dot{\gamma}_{yx} = \frac{dV_x}{dy}. \tag{2.2}$$

The force per unit area required to keep the lower plate moving at a constant velocity *V* defines the corresponding shear stress σ_{yx}, which is directly proportional to the plate velocity and inversely proportional to the distance between the plates. That is,

$$\sigma_{yx} \propto \frac{dV_x}{dy} = \dot{\gamma}_{yx} \tag{2.3}$$

The interpretation of the subscripts *yx* has been given by Bird, Stewart, and Lightfoot (2006) as follows: σ_{yx} represents a shear stress exerted in the *x*-direction on a fluid surface of constant *y* by the fluid in the region of lower *y*. It can also be interpreted as a flux of *x*-momentum transferred in the *y*-direction. The quantity on the right-hand side of Equation 2.3, $\dot{\gamma}_{yx}$, is a shear component of the rate-of-deformation tensor, $\dot{\boldsymbol{\gamma}}$, defined as

$$\dot{\boldsymbol{\gamma}} = \nabla\mathbf{V} + \nabla\mathbf{V}^{+}, \tag{2.4}$$

where $\nabla\mathbf{V}$ and $\nabla\mathbf{V}^{+}$ are the velocity gradient tensor and its transpose, respectively; $\dot{\boldsymbol{\gamma}}$ thus represents nine components.

Labeling the axes *x* and *y* is of course arbitrary. In a more general way, we can refer to the quantity on the left-hand side of Equation 2.3 as σ_{ij}, where both *i* and *j* can take on the values 1, 2, or 3. In the particular case of Cartesian coordinates, 1 refers to the *x*-direction, 2 to the *y*-direction, and 3 to the *z*-direction. σ_{ij} thus represents a quantity characterized by nine components. This quantity is a second-order tensor. We recall that a first-order tensor (or a vector) such as, for example, the velocity, requires three components to be defined (V_x, V_y, and V_z in Cartesian coordinates), and that a zero-order tensor (a scalar), such as temperature, requires only one numerical value to be completely defined.

The nine components of the stress tensor can be represented by a 3 × 3 matrix as follows:

$$\boldsymbol{\sigma} = \begin{pmatrix} \sigma_{11} & \sigma_{12} & \sigma_{13} \\ \sigma_{21} & \sigma_{22} & \sigma_{23} \\ \sigma_{31} & \sigma_{32} & \sigma_{33} \end{pmatrix}. \tag{2.5}$$

Any component of the stress tensor can be interpreted as the component of a force per unit area acting on a specific surface of a material elementary volume as depicted in Figure 2.2 for Cartesian coordinates. Let us consider surface (2), which is normal to the x_2-axis: $\underline{\boldsymbol{\sigma}}_2$ represents the net force acting on the surface per unit area; its magnitude and orientation depend on the flow field. This force per unit area is a vector that can be decomposed into three components, σ_{21}, σ_{22}, and σ_{23}.

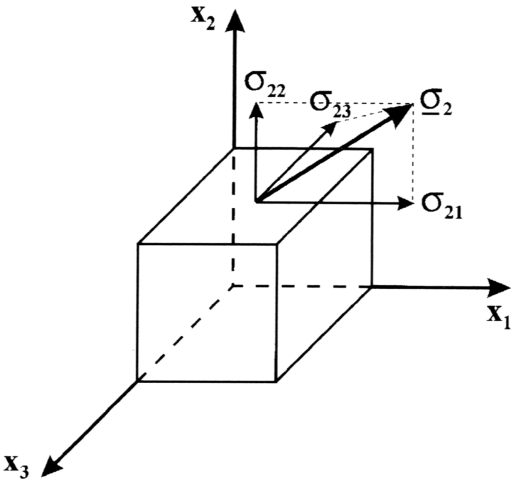

Figure 2.2
Decomposition of the force acting on a surface of a cubic element

The same procedure can be followed for the other surfaces. Since this material element is in equilibrium with its surroundings, only three resulting forces are independent, that is $\underline{\sigma}_1$, $\underline{\sigma}_2$, and $\underline{\sigma}_3$ (Lodge, 1964). Nine independent components are thus generated: the first index in σ_{ij} refers to the surface considered and the second gives the direction of the force. Finally, in equilibrium, no resultant torque can be acting on the material element: hence, $\sigma_{12} = \sigma_{21}$, $\sigma_{13} = \sigma_{31}$, and $\sigma_{23} = \sigma_{32}$ (Lodge, 1964). The stress tensor is symmetric, and this reduces the number of independent stress components from nine to six.

Of particular interest in our context (shear flow) is the component σ_{21} (the shear stress), which by symmetry equals σ_{12}, and the components σ_{ii} on the diagonal. We will be mainly interested in differences among those normal stresses, as they explain a variety of rheological phenomena. As outlined next, the shear stress σ_{21} is related to the shear rate $\dot{\gamma}_{21}$. In this context, the second subscript (1) indicates the direction of flow, and the first subscript (2) indicates the direction in which the velocity changes.

2.1.1.1 Steady-State Simple Shear Flow

For steady-shear flow, where the shear rate $\dot{\gamma}_{21}$ is constant, we define the following material functions (using $\dot{\gamma}$ for the shear rate and subscripts y and x instead of 2 and 1).

- Non-Newtonian viscosity:

$$\eta(\dot{\gamma}) = -\frac{\sigma_{yx}}{\dot{\gamma}} \tag{2.6}$$

- Primary (or first) normal stress coefficient:

$$\psi_1(\dot{\gamma}) = -\left(\frac{\sigma_{xx} - \sigma_{yy}}{\dot{\gamma}^2}\right) \tag{2.7}$$

- Secondary normal stress coefficient:

$$\psi_2(\dot{\gamma}) = -\left(\frac{\sigma_{yy} - \sigma_{zz}}{\dot{\gamma}^2}\right) \tag{2.8}$$

The quantities (σ_{xx} - σ_{yy}) and (σ_{yy} - σ_{zz}) represent the primary normal stress difference N_1 and the secondary normal stress difference N_2 respectively. The relation between ψ_1 and ψ_2 is normally taken as $\psi_2 \approx -0.1\ \psi_1$. In the majority of flow situations, the secondary normal stress coefficient ψ_2 is not all that important. Figure 2.3 to Figure 2.5 show typical viscosity–shear rate and primary normal stress difference–shear rate behavior for a variety of viscoelastic solutions, such as a 2.0 mass% solution of polyacrylamide (Separan AP 30) in a 50 mass% mixture of water and glycerine, and a 6.0 mass% solution of polyisobutylene (PIB) in Primol 355. Primol 355 is a pharmaceutical-grade white oil with a viscosity of 0.15 Pa·s at 298 K. Note the tremendous drop in viscosity over the shear rate range shown here. This behavior is typical for viscoelastic solutions. The primary normal stress coefficient data show a similar trend. However, note that the limiting behavior at low shear rates is not accessible, and that the drop with increasing shear rate is more severe in the primary normal stress difference.

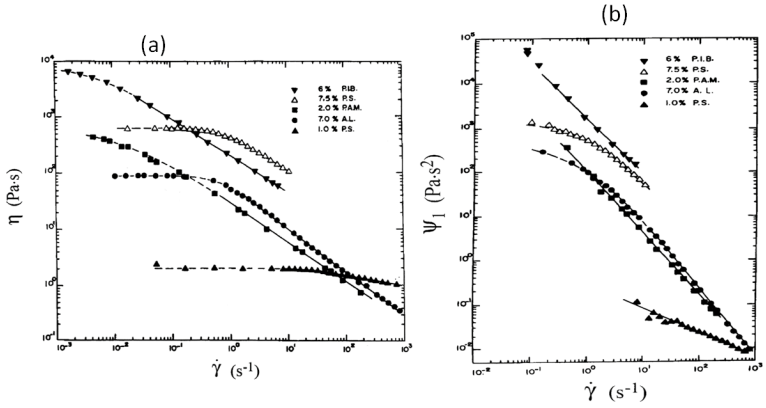

Figure 2.3 (a) Viscosity–shear rate plots and (b) primary normal stress coefficient–shear rate plots for typical viscoelastic solutions
The 1.0 and 7.5 PS are respectively 1.0 and 7.5 mass% solutions of narrow molecular weight polystyrene (M_w = 860,000 kg/kmol) in Aroclor 1248 (Data from Ashare, 1968). Aroclor 1248 is a chlorinated diphenyl with a viscosity of 0.3 Pa·s at 298 K. The 7.0% AL is a 7.0 mass% solution of aluminum laurate in decalin and *m*-cresol (Data from Huppler, 1965). The 2.0% PAM is a 2.0 mass% solution of polyacrylamide (AP30 of Dow Chemical) in a 50 mass% mixture of water and glycerine. The 6% PIB is a 6.0 mass% solution of polyisobutylene (M_w ~1.5 × 10^7 kg/kmol) in Primol 355 (Data from De Kee, 1977)

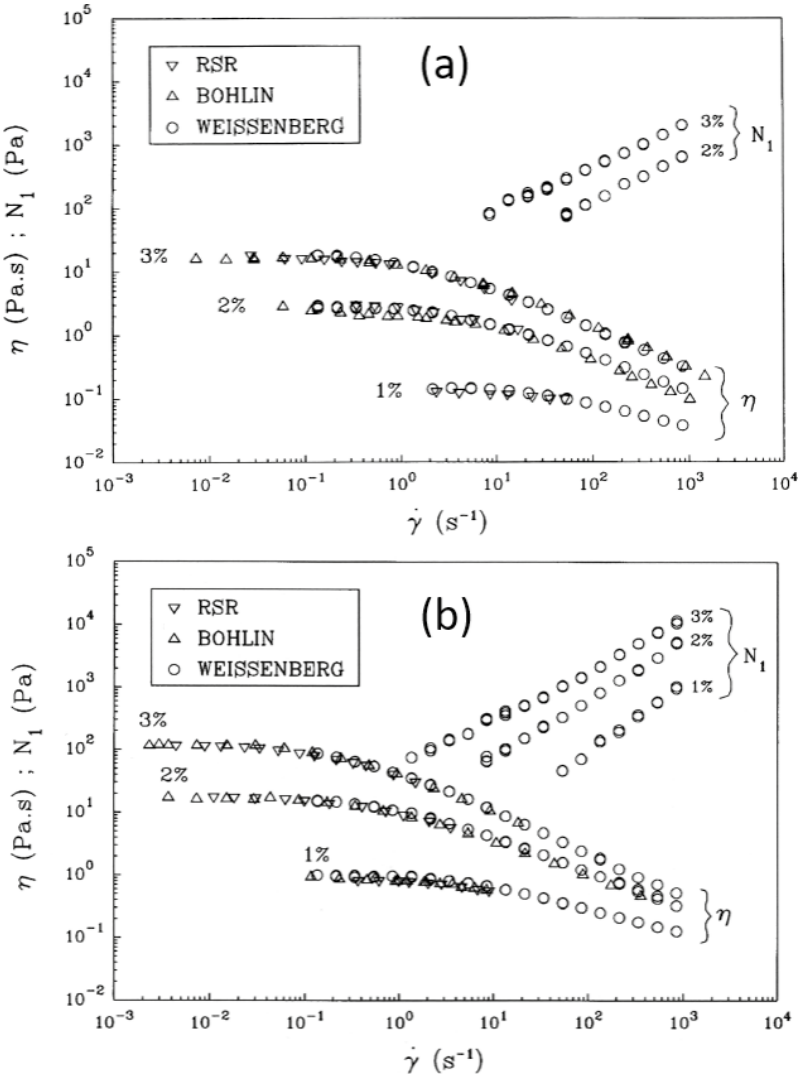

Figure 2.4 Viscosity η and primary normal stress difference N_1 versus shear rate $\dot{\gamma}$ for PEO (M_v = 1.8 × 10⁶ kg/kmol) solutions of different concentration: (a) in water (b) in a 50 mass% mixture of water and glycerine (Data from Ortiz, 1992; see Ortiz et al., 1994)

In Figure 2.4 we show typical data obtained using a Union Carbide (N-60 K) polyethylene oxide (PEO) with a molecular weight of 1.8 × 10⁶ kg/kmol for solutions of 1 to 3 mass% in water (a) and in water and glycerine (b). Shear thinning becomes more important with increasing polymer concentration. At low shear rate we can observe a zero shear rate viscosity plateau, which is more pronounced at higher concentrations. The water–glycerine solvent produces viscosities and normal stresses of a higher magnitude than the aqueous solutions. The data obtained with

different rheometers were within 15% (in the worst case) and superposed well. The three instruments used were a Weissenberg rheogoniometer, a Rheometrics (now TA Instruments) controlled stress rheometer (RSR), and a Bohlin (now Malvern) VOR rheometer.

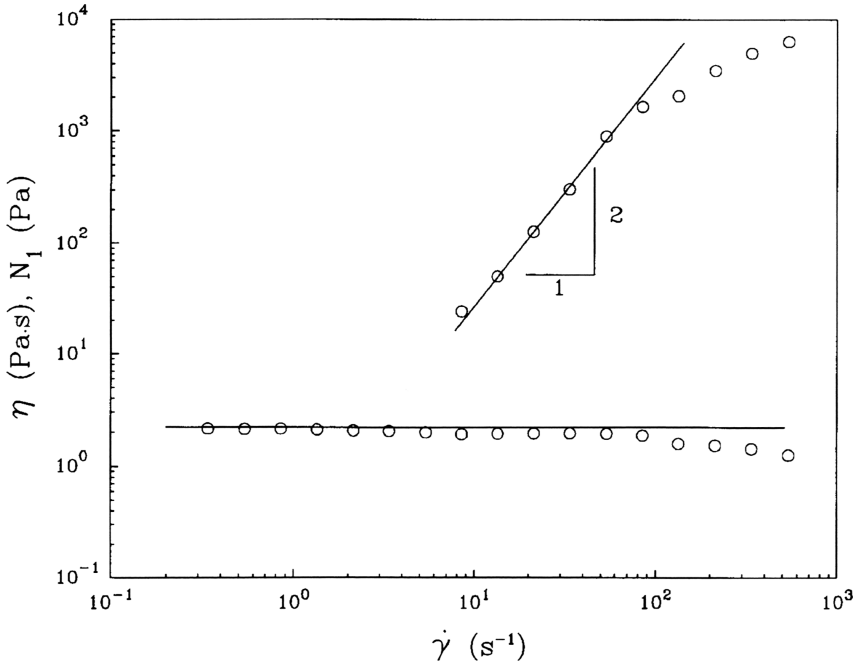

Figure 2.5 Steady-shear viscosity and primary normal stress difference of the M1 fluid at 25 °C. Data obtained on a Weissenberg rheogoniometer, model R-18

Figure 2.5 reports the steady-shear viscosity and primary normal stress difference for a so-called Boger fluid (Boger, 1977), which is a very dilute solution of a high molecular weight polymer in a very viscous solvent. The Boger fluid here is 0.244 mass% of a polyisobutylene in a mixed solvent consisting of 7 mass% of kerosene in polybutene, known as M1 (Sridhar, 1990). As shown in the figure, the viscosity is almost constant (very little shear thinning) and the primary normal stress difference is quadratic with respect to the shear rate (ψ_1 = constant) for the lower values of the shear rate. Boger fluids that are non-shear-thinning but elastic are useful model fluids for investigating rheological effects in various flow situations (Boger and Walters, 1993).

2.1.2 Sinusoidal Shear Flow

For small-amplitude oscillatory shear flow, the lower plate in Figure 2.1 would be required to oscillate sinusoidally in the x-direction, with small amplitude, with a range of frequencies ω. This situation is illustrated in Figure 2.6. In this case, we define a complex viscosity as follows:

$$\eta^* = \eta' - i\eta'' = -\frac{\sigma_{21}^0}{\dot{\gamma}^0}, \tag{2.9}$$

with

$$\dot{\gamma}(t) = \mathrm{Re}\left[\dot{\gamma}^0 \, \mathrm{e}^{i\omega t}\right] \tag{2.10}$$

and

$$\sigma_{21}(t) = \mathrm{Re}\left[\sigma_{21}^0 \, \mathrm{e}^{i\omega t}\right]. \tag{2.11}$$

For small deformation (in the linear viscoelastic domain as discussed in Chapter 5), inertial effects can be ignored, and the stress response is a sine wave of the same frequency as the input function, but out of phase. Here Re[–] stands for the real part of [–]; $\dot{\gamma}^0$ and σ_{21}^0 represent the complex amplitudes of $\dot{\gamma}$ and σ_{21} respectively; η' is referred to as the dynamic viscosity and is associated with energy dissipation (due to viscous effects); while the coefficient of i, η'', represents an elastic contribution associated with energy storage, and which could be labeled dynamic rigidity.

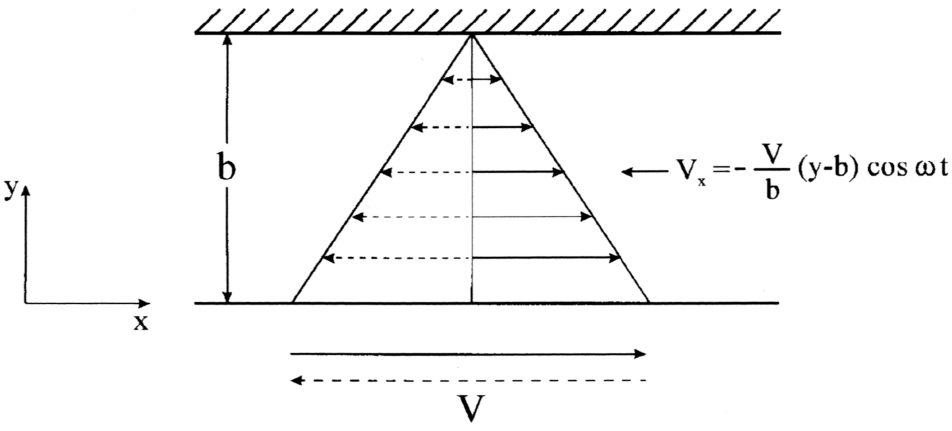

Figure 2.6 Sketch defining sinusoidal shear flow

It is also possible to work in terms of a quantity G^*, defined as

$$G^* = G' + iG'', \tag{2.12}$$

where the storage modulus $G' = \omega\eta''$ and the loss modulus $G'' = \omega\eta'$. These material functions are used for material characterization, and they relate to molecular structure (Ferry, 1980).

Figure 2.7 illustrates the dependence of the dynamic viscosity η' and the storage modulus G' on the frequency ω, for 3.0 mass% PEO solutions of different molecular weights. We observe that at a given frequency, ω, both η' and G' increase with molecular weight, and at high frequency they both approach a simple power-law behavior, almost independent of the molecular weight of the polymer.

From another vantage point, small-amplitude oscillatory (SAOS) data are usually reported in terms of the norm of the complex viscosity $\left|\eta^*\right|$, storage modulus (G'), or loss modulus (G''), in each case as a function of the radial frequency. For simplicity, the bars in the norm of the complex viscosity are frequently omitted, to write simply η^*.

Figure 2.8 reports the complex viscosity and the storage modulus as functions of the angular frequency of three polymer melts, namely, a high molecular weight polylactide (HPLA), a low molecular weight polylactide (LPLA) and a poly[(butylene adipate)-co-terephthalate] (PBAT) at 160 °C. The behavior is typical of homogeneous polymer melts with the complex viscosity, exhibiting a plateau at low frequencies and a rapidly decreasing value at high frequencies (shear thinning). The storage modulus (Figure 2.8b) is seen to increase with frequency, with an initial slope of 2 (log–log scales), corresponding to a so-called terminal zone.

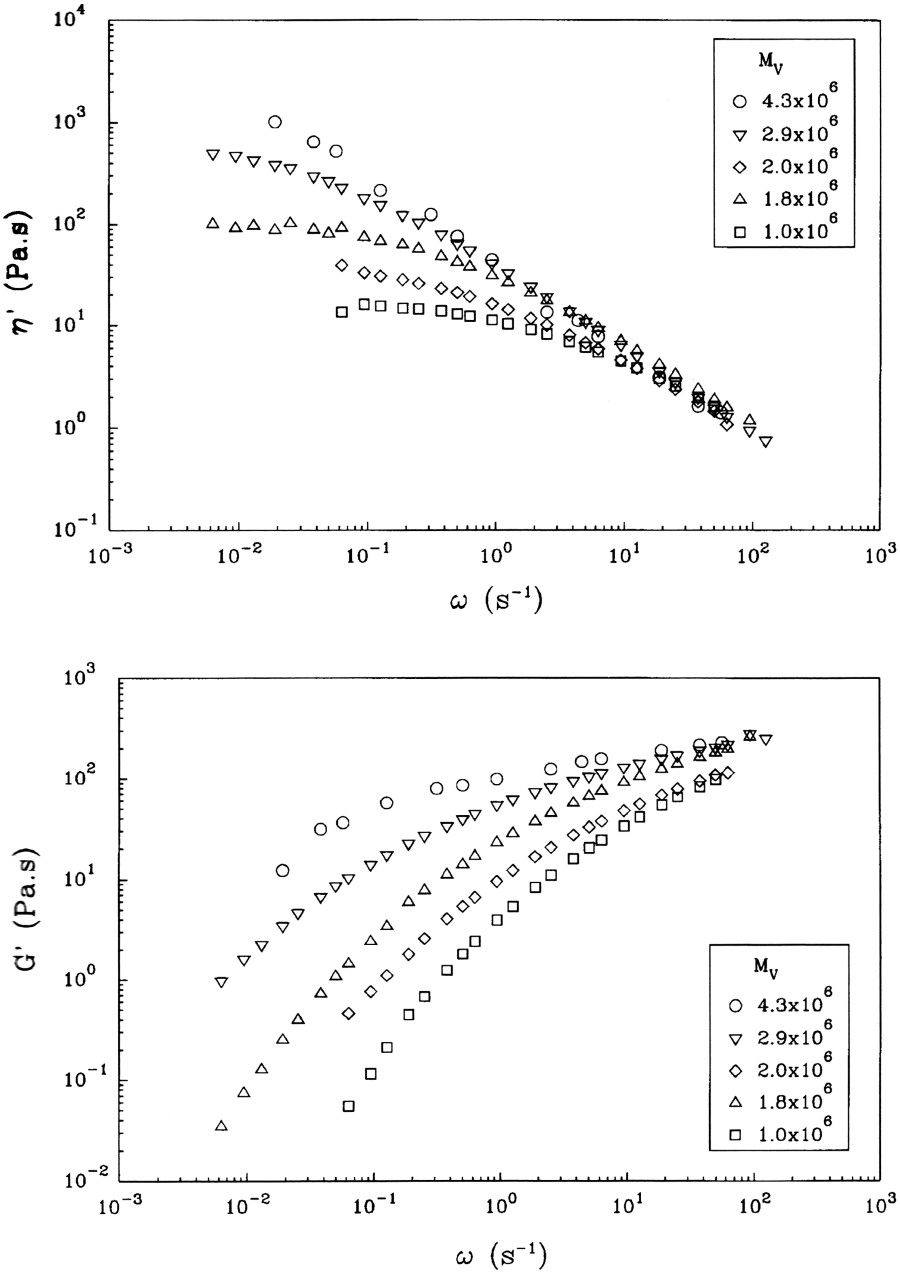

Figure 2.7 Effect of the viscosity-average molecular weight (M_v) on the dynamic data for 3 mass% PEO solutions in water and glycerine:
(a) η' data
(b) G' data
(Data from Ortiz, 1992 (see Ortiz et al., 1994))

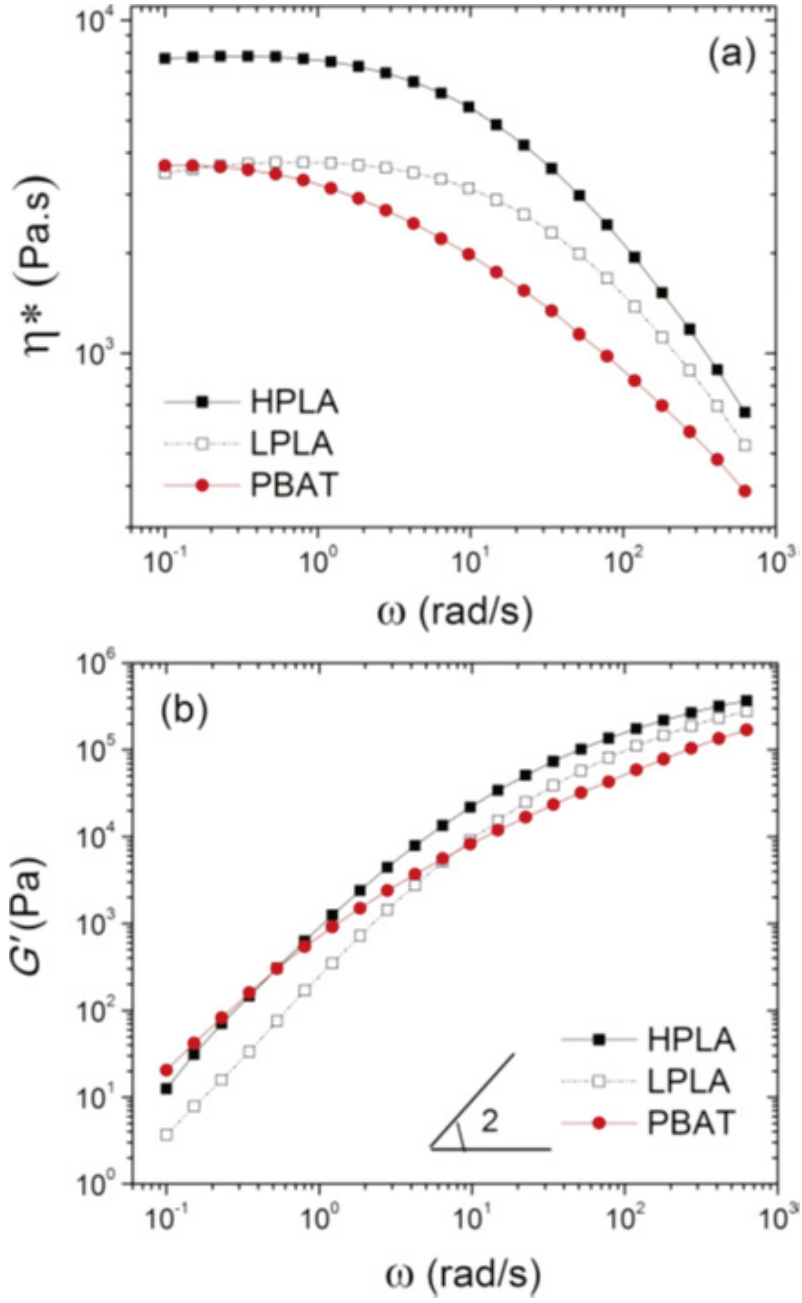

Figure 2.8 (a) Complex viscosity, η^* and (b) storage modulus, G', as functions of angular frequency, ω, for three molten commercial polymers: a high molecular weight polylactide (HPLA), a low molecular weight polylactide (LPLA) and a poly[(butylene adipate)-co-terephthalate] (PBAT) at 160 °C (from Nofar et al., 2016)

2.1.3 Transient Shear Flows

Transient or time-dependent shear flows are associated, for example, with the start-up of processes involving the displacement of viscoelastic materials. Under such initial flow conditions, stresses can reach magnitudes which are substantially larger than their steady-state values achieved for the applied shear rate.

2.1.3.1 Stress Growth Experiment

For stress growth, after onset of steady simple shear (the lower plate in Figure 2.1 starts moving in the positive x-direction), we have

$$\dot{\gamma}(t) = \dot{\gamma}_\infty h(t), \tag{2.13}$$

where $\dot{\gamma}_\infty$ is the constant velocity gradient for $t > 0$, and $h(t)$ is the unit step function

$$h(t) = 0 \quad \text{for} \quad t < 0 \tag{2.14}$$

and

$$h(t) = 0 \quad \text{for} \quad t > 0 \tag{2.15}$$

We define the time-dependent shear stress and normal stress coefficients as follows:

$$\eta^+(t, \dot{\gamma}_\infty) = -\frac{\sigma_{yx}(t)}{\dot{\gamma}_\infty}, \tag{2.16}$$

$$\psi_1^+(t, \dot{\gamma}_\infty) = -\frac{[\sigma_{xx}(t) - \sigma_{yy}(t)]}{\dot{\gamma}_\infty^2}, \tag{2.17}$$

and

$$\psi_2^+(t, \dot{\gamma}_\infty) = -\frac{[\sigma_{yy}(t) - \sigma_{zz}(t)]}{\dot{\gamma}_\infty^2}. \tag{2.18}$$

Figure 2.9 illustrates this experiment schematically. The lower part of the figure shows the effect of the imposed shear rate $\dot{\gamma}_\infty$ on the reduced shear stress growth function. $\eta(\dot{\gamma}_\infty)$ is the steady-shear viscosity value. At low $\dot{\gamma}_\infty$, the function increases monotonically. At higher values of $\dot{\gamma}_\infty$, stress overshoot occurs. The time at which the maximum overshoot occurs decreases with increasing shear rate, and the magnitude of the overshoot increases with increasing shear rate. The higher the shear rate, the sooner steady state is attained. The response of a Newtonian fluid (η^+/η), in the absence of inertial effects, is given by the unit step function.

Index

D

E

F

G

H

M

N

O

P

R

U

V

W

Y